International Journal of Biological Macromolecules 245 (2023) 125482

Contents lists available at ScienceDirect

International Journal of Biological Macromolecules

journal homepage: www.elsevier.com/locate/ijbiomac

Carbon dots, cellulose nanofiber, and essential oil nanoemulsion from *Torreya grandis* aril added to fish scale gelatin film for tomato preservation

Junjun Bao [a,1], Yuanyuan Hu [a,1], Mohamed A. Farag [b], Weiwei Huan [a], Jiasheng Wu [a,*], Dapeng Yang [c,*], Lili Song [a,*]

[a] State Key Laboratory of Subtropical Silviculture, Zhejiang A&F University, Lin'an 311300, Zhejiang Province, People's Republic of China
[b] Pharmacognosy Department, College of Pharmacy, Cairo University, Kasr el Aini st., 16, Cairo P.B. 11562, Egypt
[c] College of Chemical Engineering and Materials Science, Quanzhou Normal University, Quanzhou 362000, China

ARTICLE INFO

Keywords:
Torreya grandis aril waste
Nanomaterials
Functional composite film

ABSTRACT

In this study, carbon dots (CDs), cellulose nanofibers (CNF) and essential oil nanoemulsion (EON) were extracted from the aril waste of *Torreya grandis* following nuts production. These three nanomaterials were formulated for the preparation of a composite film to be employed for postharvest tomato storage. Visual, microscopical and physicochemical properties of the prepared nanocomposite films were analyzed at different levels of CDs and CNF for optimization purposes. The UV absorption and antioxidant capacity of gelatin film with 10 % CDs (G/10CD) were enhanced compared with gelatin (G) film, concurrent with a reduction in water barrier capacity, water contact angle (WCA) and tensile strength (TS). Compared with G/10CD film, the WCA of G film after incorporation of 10 % CDs and 3 wt% CNF (G/10CD/3CNF) was significantly increased by 14.5°at 55 s. In contrast, TS increased by 1.26 MPa, as well as the significant enhancement in water barrier capacity. The above composite film mixed with EON (G/10CD/3CNF/EON) exerted further antimicrobial effects against *Escherichia coli*. G/10CD/3CNF/EON coating effectively extended tomato shelf life compared with the control group. Therefore, this new eco-friendly film presents several advantages of biodegradability, sustainability as well as multifunctional properties posing it as potential packaging material for food applications.

1. Introduction

Nowadays, the increasing consumption of plastic packaging in food industry is posing a potential threat to the environment owing to its low recylability and degradation [1]. Hence, research on developing new green packaging materials have attracted increasing attention in recent years to aid replace some plastic packaging and mitigate against associated environmental problems.

Several studies reported that several nature-derived biopolymers can be used as base formulation for packaging, such as proteins [2], polysaccharides [3,4] and lipids [5], due to their sustainability and high biodegradability [6]. Among these biopolymers, gelatin is a kind of protein, which is a hydrophilic colloid partially hydrolyzed by collagen, and widely abundant in mammalian skin and bone such as cow, pig *etc.* [7]. It has been reported that fish scales are rich in gelatin but are mostly discarded, with *ca.* 7.32 million metric tons of fish scales discarded each year [8], posing it as major source for gelatin extraction among dietary sources [9]. Although gelatin has been widely used as a food-protection film, it has limited application due to its poor water barrier capacity, mechanical properties, and weak antibacterial activity [10]. Therefore, improvement of gelatin functionalities is ongoing by designing it with other materials, such as nanomaterials [11].

Carbon dots (CDs), as a zero-dimensional carbon nanoparticles, are known for their low toxicity, photoluminescence, and biocompatibile properties [12]. In addition, it has been reported that CDs have excellent *in vitro and in vivo* free radical scavenging activities, to be used as antioxidants [13]. Cellulose nanofibers (CNF) are considered non-toxic, with high surface area and aspect ratio, and are used as a support filler to improve film mechanical properties [14,15]. Several studies have been reported on film anti-bacterial activity posing it as potential food packaging material [16,17]. Recently, synthetic chemical preservatives become increasingly replaced by natural essential oil as a natural antimicrobial agent [18]. However, limitation of essential oils employment in food packaging is attributed to its volatility and hydrophobicity [19].

* Corresponding authors.
E-mail addresses: wujs@zafu.edu.cn (J. Wu), yangdp@qztc.edu.cn (D. Yang), lilisong@zafu.edu.cn (L. Song).
[1] These authors have contributed equally to this work.

https://doi.org/10.1016/j.ijbiomac.2023.125482
Received 25 March 2023; Received in revised form 9 June 2023; Accepted 17 June 2023
Available online 20 June 2023

In practice, essential oils were added with active agents to form essential oil nanoemulsion (EON) by homogenization to improve its functional properties [20]. The gelatin film based on CDs and CNF through incorporation of EON and assessment of its antimicrobial properties has yet to be reported in literature.

Torreya grandis, belonging to the genus *Torreya* of Taxaceae, is a unique economic tree species in Southern China. The nut exhibits high nutritional value due to its richness in unsaturated fatty acid such as sciadonic acid [21]. *T. grandis*, the green arils of nuts accounts for 50 % of the whole fruit composition. Studies have confirmed that aril is rich in cellulose, phenolics, flavonoids, and essentail oil [22]. Although only a small amount of arils are used for essential oil extraction, most of which are discarded following nuts production leading to environmental problems asides from wasting such valuable resource [23].

Consideration arils richness in cellulose and essential oil, this study aimed to assess: 1) successfully extract the nanomaterials (such as CDs, CNF, EON) from arils waste; 2) designing gelatin composite film based on CDs, CNF and EON; 3) application potential of the new composite films to be used as eco-friendly packaging material for fruit preservation. For optimization purposes, the water barrier capacity, microstructure, thermal stability, mechanical and antimicrobial properties of the composite films were investigated when incorporation of CDs, CNF and EON. In addition, the effect of the composite film on the physiological parameters of tomato during postharvest stage were assessed for proof of application in food industry. This study aids to provide eco-friendly sustainable material for fruit packaging based on unexploited resources such as Torreya nut aril for the first time in literature.

2. Experimental section

2.1. Materials

The aril waste of *Torreya grandis* were collected from Zhejiang A&F University, Hangzhou, Zhe jiang province, China. The discarded fish scales and tomatoes were purchased from Xinhuadu Supermarket (Quanzhou, China). *Escherichia coli* was provided by the second hospital of the Fujian Medical University, Quanzhou, Fujian province, China. All other chemicals were of analytically grade and purchased from Sinopharm Chemical Reagent Co, Ltd. (Shanghai, China). Ultra-pure water was used as solvent (Sichuan Youpu Instrument and Equipment Co., Ltd., Sichuan, China).

2.2. Preparation of carbon dots (CDs)

CDs were fabricated using a one-step hydrothermal method (Scheme 1). The arils of *T. grandis* were crushed using a high-speed sample grinder (JP-500C, Yongkang Jiupin industry and trade Co. Ltd., Jinhua City, Zhejiang province, China). The powder (2 g) was refluxed with 30 mL of ultrapure water in a polytetrafluoroethylene reactor. The mixture was refluxed at 180 °C reaction for 8 h, left to cool to room temperature. After separation of the residue by filteration using filter paper (diameter 12.5 cm), followed by 0.22 μm nylon glass fiber filter membrane, a yellow transparent solution of CDs was obtained.

2.3. Preparation of cellulose nanofibers (CNF)

CNF were prepared by a slightly modified procedure [24]. *T. grandis* aril powder (10 g) was mixed with 500 mL 4 % NaOH at 80 °C for 4 h, washed with 0.2 M phosphate buffer (pH 6.8) to neutralize, bleached with 2 % sodium chlorite and acetic acid buffer for 4 h, and the bleached sample was filtered and washed with phosphate buffer (pH 6.8), The cellulose nanofiber gel was then prepared using acid hydrolysis with 65 wt% H_2SO_4, heating at 60 °C and mechanical agitation for 2 h. Reaction was terminated by the addition of cold water, filtering out excess acid, adjusting pH to 6.8, and ultrasonic dispersion for 1 h.

2.4. Preparation of essential oil nanoemulsion (EON)

EON was obtained by adding surfactant Tween 80 and homogenization using microjet homogenizer (NANO, NOOZLE, USA). 2.5 g of Tween 80 and 92.5 g deionized water were mixed with 5 mL pure essential oil and homogenized for 20 min.

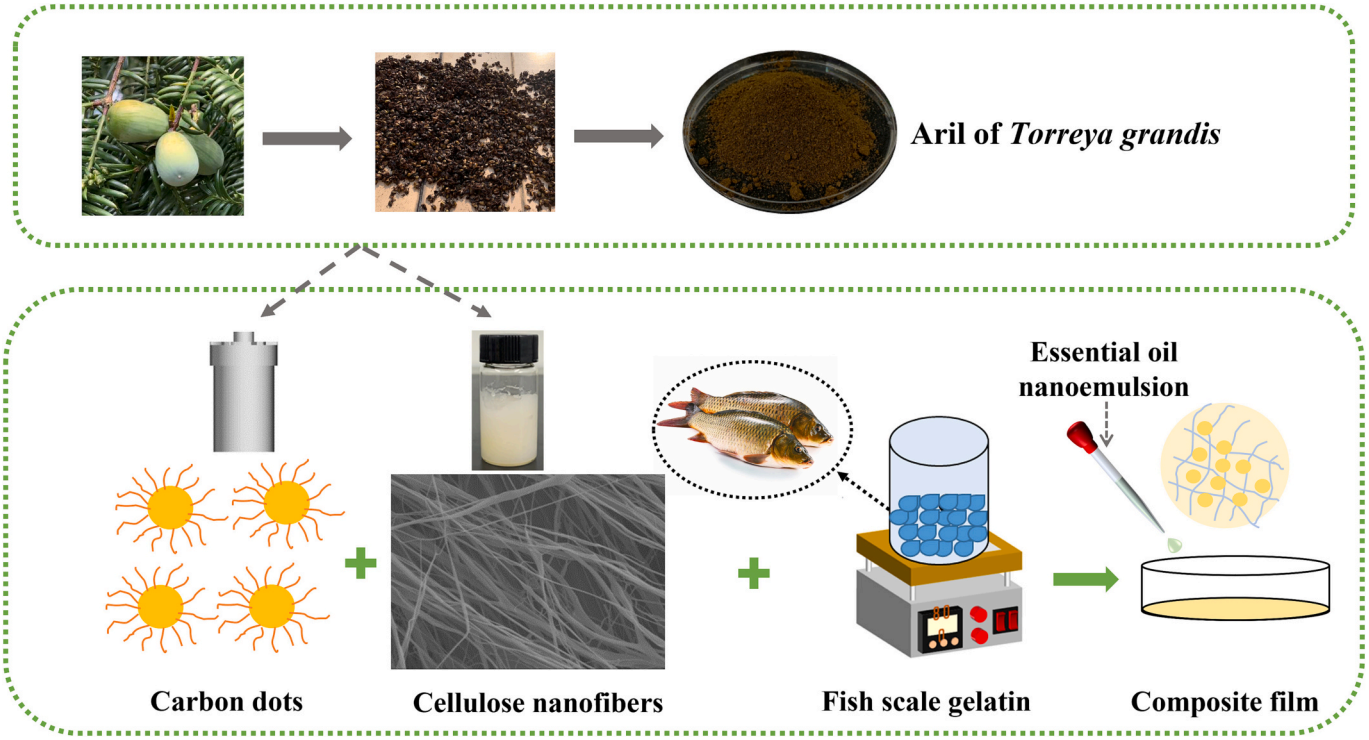

Scheme 1. Introduction to the preparation process of composite membranes.

2.5. Characterization of nanomaterials

2.5.1. Physical structure

The CDs were diluted with deionized water (9:1) and their UV–vis absorption spectra were recorded using a UV–vis spectrophotometer (Analytic Jena, Specord S600, Germany). The fluorescence spectrum was obtained using FL970 fluorescence spectrophotometer (Techcomp, Shanghai, China). The morphology of CDs and EON were observed using by transmission electron microscopy (TEM) with an equipment Tecnai F30 electron micoscopy with a voltage of 300 kV, and Image J was used to calculate the particle size distribution. CNF topography was observed using scanning electron microscopy (SEM, Zeiss, Germany) and the size of CNF was measured by Nano 2S90 particle sizer (Malvern, UK).

2.5.2. Chemical structure

The crystal structure of CNF and aril was analyzed at the 2θ degree using X-ray diffractometer (XRD, Bruker D8 Advance, Germany). The scanning angle ranged from 10° to 90°, radiated by Cu Kα. Both CNF and aril were cut into small pieces and put under probe, the wavelengths were recorded using fourier transform infrared spectroscopy (FTIR, Thermo Scientific, USA) scanning from 500 to 4000 cm^{-1}, with a resolution of 4 cm^{-1} and scanning rate of 120 times per min.

2.6. Preparation of composite membranes

The scale gelatin/carbon dots/cellulose nanofibers composite films were prepared using the solution casting method [25]. Briefly, 40 g of fish scale was treated with 0.6 M HCl for 15 min to remove $CaCO_3$ and washed with phosphate buffer (pH 6.8). Then, 300 mL distilled water was added to fish scale and boiled for 3 h followed by filteration to remove residue yielding a fish scale gelatin solution. Glycerin was added at 1: 0.5 *v*/v and cross-linked by magnetic stirring at 1000 rpm for 20 min. 20 mL solution was poured into a plate of diameter 9 cm, dried at 37 °C using DHG-9240A air blower for 24 h, and served as a blank control (G, gelatin). Various concentrations of CDs (5 %, 10 %, 15 %, 20 %) were added into gelatin glycerin by continuous stirring and mixing, termed as G/5CD, G/10CD, G/15CD, G/20CD, respectively. Base on the best addition amount of CDs, different proportions (3, 5, 7 wt%) of CNF was added to G/10CD, termed as G/10CD/3CNF, G/10CD/5CNF and G/10CD/7CNF, respectively. G/10CD/3CNF, then mixed with 1 mL of 5 % essential oil nanoemulsions (EON), termed as G/10CD/3CNF/EON (Scheme 1). All the mixtures likewise poured into a plate with a diameter of 9 cm and dried in at 37 °C using air blower for 24 h.

2.7. Characterization of G/CD films

2.7.1. Thickness

Film thickness was measured with a digital micrometer IP65 (Songqi Technology Co., Ltd., China), and each film was measured at 8 different points, with the average value calculated and expressed as mm.

2.7.2. Color measurement

The colorimetric index of the film sample (4 × 1 cm) was recorded using a colorimeter with pulsed xenon lamp (CR400, Konica Minolta, Inc., Japan), including L*(lightness), a* (+ redness, − greenness), b* (+ yellowness, − blueness), and total color difference ΔE was calculated using the Eq. (1).

$$\Delta E = \sqrt{(L^* - L_0)^2 + (a^* - a_0)^2 + (b^* - b_0)^2} \quad (1)$$

where L_0, a_0, b_0 are parameters to the whiteboard. ($L_0 = 93.45$, $a_0 = -0.81$, $b_0 = 0.33$).

2.7.3. UV–visible absorbance and transmittance.

To evaluate film performance to shield the transmission of ultraviolet and visible light (UV–vis), its transmittance and absorbance were measured at 200–800 nm using an ultraviolet spectrophotometer (Jena specord S600, Germany). The G film with different proportions of carbon dots were cut into 1 × 4 cm strips and placed outside quartz cuvette to obtain the absorption and transmission curves in UV–vis region, respectively.

2.7.4. In vitro Antioxidant activity

2.7.4.1. DPPH method. The composite films were cut into a 5 mm diameter disc using a punch, and five pieces were added to 3 mL DPPH-ethanol solution (0.02 mM), shaken, and mixed well. Mixture was then stored in the dark to react for 30 min, and absorbance was measured at 517 nm. The pure gelatin prepared under the same conditions was treated as a blank. The radical clearance was calculated as follows:

$$\text{Scavenging activity} = \frac{A_0 - A_1}{A_0} \times 100\% \quad (2)$$

where A_0 is the absorbance of the pure gelatin sample, A_1 is the absorbance of the composite film sample.

2.7.4.2. ABTS method. To obtain the ABTS solution, ABTS (7.4 mM) and $K_2S_2O_4$ (2.6 mM) were mixed, and left to react in the dark for 12 h, further diluted with 100 % ethanol. Then, the ABTS solution was diluted until the absorbance reached 0.7. The sample sizes were similar to DPPH assay, five samples were added to 3 mL ABTS solution, incubated in the dark for 1 h, and the mixture was taken to measure its absorbance at 734 nm. The radical clearance was calculated using same equation as DPPH method.

2.8. Characterization of G/CD/CNF films

2.8.1. Scanning electron microscopy (SEM)

The surface morphology of composite films was observed by SEM (Zeiss, Germany). The composite film samples were pasted on the conductive adhesive, and after gold spraying, surface and cross-section morphology of the composite film were observed by magnifying 200 times at 2 KV high voltage.

2.8.2. X-ray diffraction (XRD)

The crystal structure of the composite film was analyzed by the same method reported in Section 2.5.2.

2.8.3. Fourier transform infrared spectroscopy (FTIR)

All film samples were cut into small pieces and put under probe, the wavelength of CNF and three composite films were recorded by the same method in Section 2.5.2.

2.8.4. Moisture content (MC) and water solubility (WS)

The weight of the film stored at 25 °C is recorded and then it is dried to constant weight to 60 °C using a blast drying oven, the MC of films were calculated and expressed as relative weight (%).

2 × 2 cm dried film samples were placed in a glass bottle, 15 mL distilled water was added followed by stirring using a magnetic stirrer at 100 rpm. The insoluble parts were separated onto pre-weighed filter paper W_1, kept at 60 °C and the weight was recorded as W_2 after drying. Water solubility was calculated using the following formula:

$$\textit{Water solubility}\ (\%) = \frac{W_1 - W_2}{W_1} \times 100\% \quad (3)$$

2.8.5. Water contact angle

The 1 × 1 cm film was placed on a flat contact angle measuring platform JY-PHb (Jinhe Instrument Manufacturing Co., Ltd., Hebei, China), and a syringe was used to drip 10 μL of deionized water. A camera was used to record the changes in contact angle within one minute, once in every five seconds. The average water contact angle was

measured using Image J software.

2.8.6. Water vapor permeability (WVP)

15 mL of deionized water was packed into a glass tube with a diameter of 25 mm and a depth of 55 mm. The composite film was sealed at the mouth of the glass and placed in a silica gel dryer. The weight was recorded every 12 h and measured continuously for one week on a regular time intervals, the slope was calculated using linear regression equations. WVTR and WVP were calculated using these equations.

$$WVTR = \frac{slope}{s} \tag{4}$$

$$WVP = WVTR \times L/\Delta P \tag{5}$$

where s denotes membrane area, L is the thickness of the membrane, ΔP is the vapor pressure difference inside and outside the bottle.

2.8.7. Thermal properties

TGA (Q50, America) was used to evaluate the thermal stability of the membrane. Under the nitrogen atmosphere, the heating range was set from 25 to 600 °C, with heating rate at 10 °C/min.

2.8.8. Mechanical properties

The mechanical properties of composite membranes were tested on a universal testing machine (INSTRON, USA). The composite films were cut into 60 × 15 mm rectangles, where one side of the fixture is fixed, and the other side is stretched at a speed of 50 mm/s, with an initial distance of 20 mm. Tensile strength (TS) and elongation at break (EBA) were calculated using the following equations.

$$\text{TS (MPa)} = \frac{F_{max}}{\text{A}} \tag{6}$$

$$\text{EBA (\%)} = \frac{\text{L} - L_0}{L_0} \times 100 \tag{7}$$

where F_{max} is the maximum tensile strength (N), A is the area of the film (mm^2), and L is the (mm), L_0 is the (mm).

2.9. Antimicrobial properties

Bacteriostatic activity was assessed using plate counting method [26]. The 1 mL *E. coli* bacteria (10^6 CFU/mL) was mixed with 20 μL composite membrane solution, placed on a shaker for 2 h, 3 h, 4 h, 5 h, respectively, 20 μL mixture was coated on a plate, and incubated at 37 °C for about 18 h. The bacteriostatic effect of the composite membrane was assessed as colony number after incorporation of EON within 5 h.

2.10. Preservative effect of composite membrane on tomato fruits

The composite film was coated on the surface of the fruit as a coating before the film is formed. Water was set as blank control, pure gelatin film, and composite film treatment, with each treatment to include *ca.*100 fruits. The tomatoes were immersed in the liquid for one min, taken out, dried at 26 °C and soaked again. This process was repeatedly twice and further kept separately in a plastic bag stored in a thermostat incubator at 28 °C with 40 % humidity. The appearance and physiological indexes of tomatoes were observed for a week.

2.10.1. Color parameters

The method is the same reported in Section 2.7.2.

2.10.2. Firmness

Tomato firmness was measured using a GY-1 fruit firmness meter (Sundoo, Wenzhou, China). The average value of 9 fruits was determined for each treatment.

2.10.3. Soluble solids content (SS) and titratable acidity (TA)

Tomato fruit was homogenized for 10 min, and supernatant was aliquoted, and one drop was placed inside a refractometer (Atago, Japan) to determine soluble solids and titratable acids (Atago, Japan).

2.11. Statistical analysis

SPSS 23 was used for statistical analysis using one-way ANOVA and Tukey pot hoc test ($P < 0.05$). Origin 2018 (Origin Lab, Northampton, CA, USA) was used as the mapping software.

3. Results and discussion

3.1. Characterization of nanomaterials

TEM image examination revealed that CDs were uniformly distributed, with a diameter of *ca.* 5.2 nm (Fig. 1a-b). The TEM image showed that essential oil was distributed as nano-sized particles, with droplet size of *ca.* 12.5 nm (Fig. 1c-d), which can protect essential oil from volatilization [27]. Fig. 1 c showed SEM image of the cellulose nanofibers after acid and alkali treatment ranging in diameter between 10 and 100 nm (Fig. 1e-f).

In addition, UV visible absorption spectra analysis showed an absorption peak at 298.5 nm (Fig. 2a), likely attributed to n - π * transition of C—O and C—C * transition [28]. The inset in Fig. 2a showed that CDs were brownish yellow under normal light and to fluoresces blue under UV light. From the fluorescence spectrum (Fig. 2b), it can be seen that CDs exhibited strongest emission peak at 428 nm upon excitation at 351 nm UV light. There appeared to be a red-shift of CDs upon change in excitation wavelength from 280 nm to 480 nm (Fig. 2c), caused by the change of the electron gap [29]. The fluorescence intensity of CDs decreased with the increasing CDs dose (Fig. 2d).

Compared with aril, the band at 3420 cm^{-1} in CNF became lower, concurrent with the disappearance of the band at 1723 cm^{-1} (Fig. 2e) attributed to the O—H and acetyl and uronic ester groups in lignin and hemicellulose [30]. In addition, our XRD result showed two typical peals at 15.8° and 22.2° indicating the presence of cellulose I structure [31]. These results imply that cellulose nanofibers (CNF) was successfully achieved after the efficient removal of lignin and hemicellulose.

3.2. Characterization of G/CD films

The appearance of film is always reflected by its color, and to affect consumer's preferences [32]. The optical properties of film were listed in Table 1. G film had the highest L* value (lightness) *versus* the lowest a*(redness/greenness), b*(yellowness) and ΔE values, compared with composite films as well as CDs film. Both the lightness and redness/greenness declined within increase of CDs percentage in the composite films. The yellowness of the film increased continuously by 10 % addition of CDs and remained steady at that level. The trends of color difference were similar to the L* and a* values. The lower L* value and the higher a* value of G/CD films were mainly attributed to their decreasing light transmission [33].

Photo-oxidation and photo-damage contributed towards food oxidation and or deterioration [34]. In practice, light-induced damage can be alleviated upon packaging with the composite films [35]. In the present study, UV band at 240–330 nm increased with increase of CDs percentage in the composite films (Fig. 3a), indicating that the films enhanced UV absorption and blocked UV radiation with addition of CDs (Fig. 3a). In addition, the lower transmittance in the visible range was observed at the composite CDs films (Fig. 3b), which was consistent with report of Wang et al. (2020) that CDs-based composite film led to a decrease in UV transmittance [36].

The addition of CDs to gelatin films, as a functional material is expected to enhance films antioxidant property and protect foods from oxidative damage [37]. The free radical scavenging rate depends on the

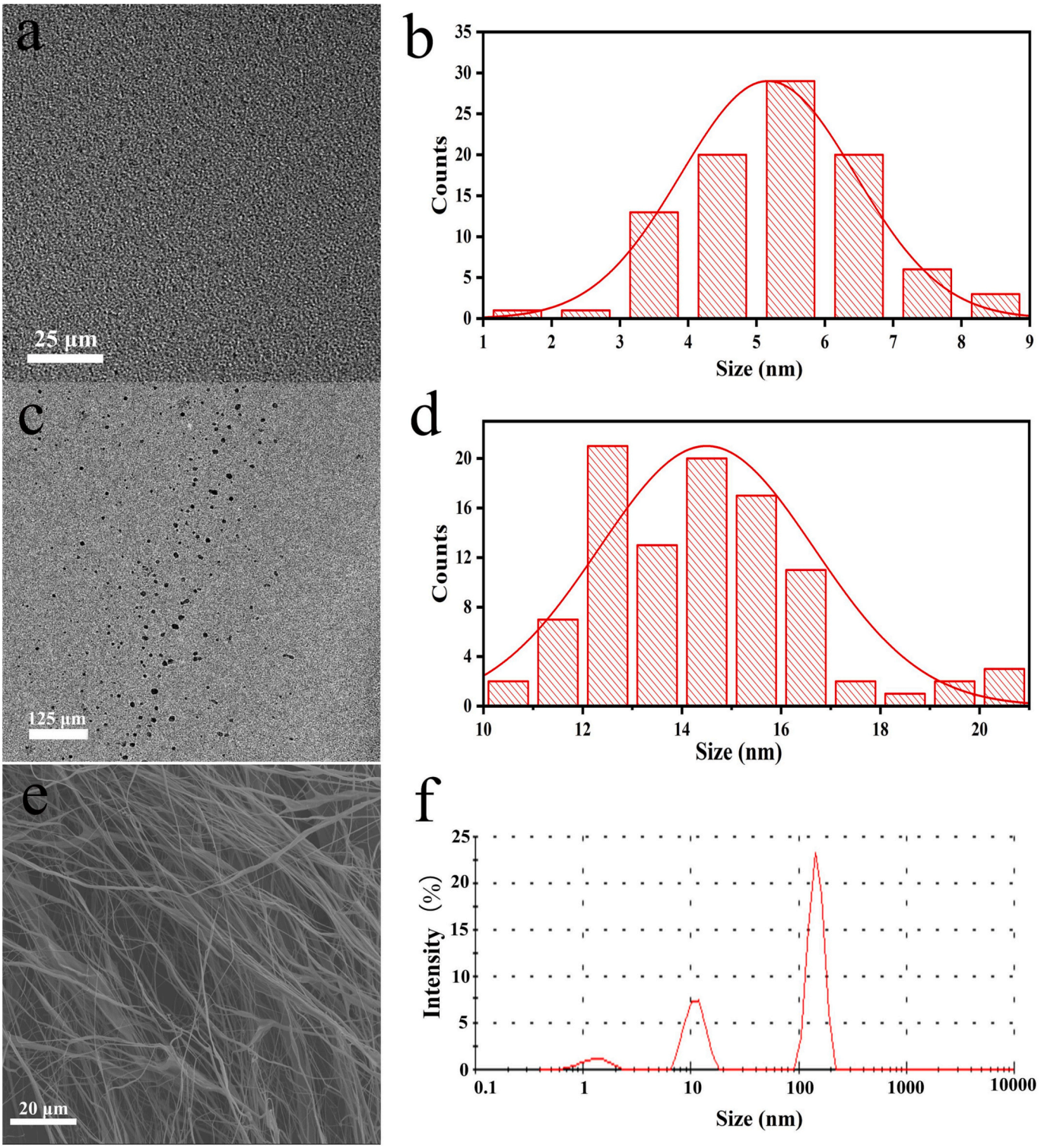

Fig. 1. Transmission electron microscopy (TEM) image and particle size of CDs (a-b) and NEO (c-d), and scanning electron microscopy (SEM) image and size of CNF (e-f).

antioxidant level attributed to the surface-rich -OH, -NH_3, and -COOH [38]. Results of DPPH and ABTS radical scavenging assays of composite film at different CDs levels are shown in Fig. 3c-d. The DPPH radical scavenging activity was 60 % and 80 % at 5 % CDs and 10 % CDs, respectively, with DPPH radical scavenging activity to show no further increase beyond 10 % CDs addition. The ABTS scavenging activity of the film increased continuously with increase in CDs level. Therefore, 10 % CDs was selected as optimum dose in the further studies of the composite film with cellulose nanofibers.

3.3. Appearance and thickness of G/10CD/CNF films

As shown in Fig. 4a-e, all five film types showed high transparency. Pure gelatin film is transparent and colorless, G/10CD film is yellow and transparent, and the surface is smooth. Cellulose nanofibers (CNF) is insoluble and uniformly dispersed inside the membrane, without

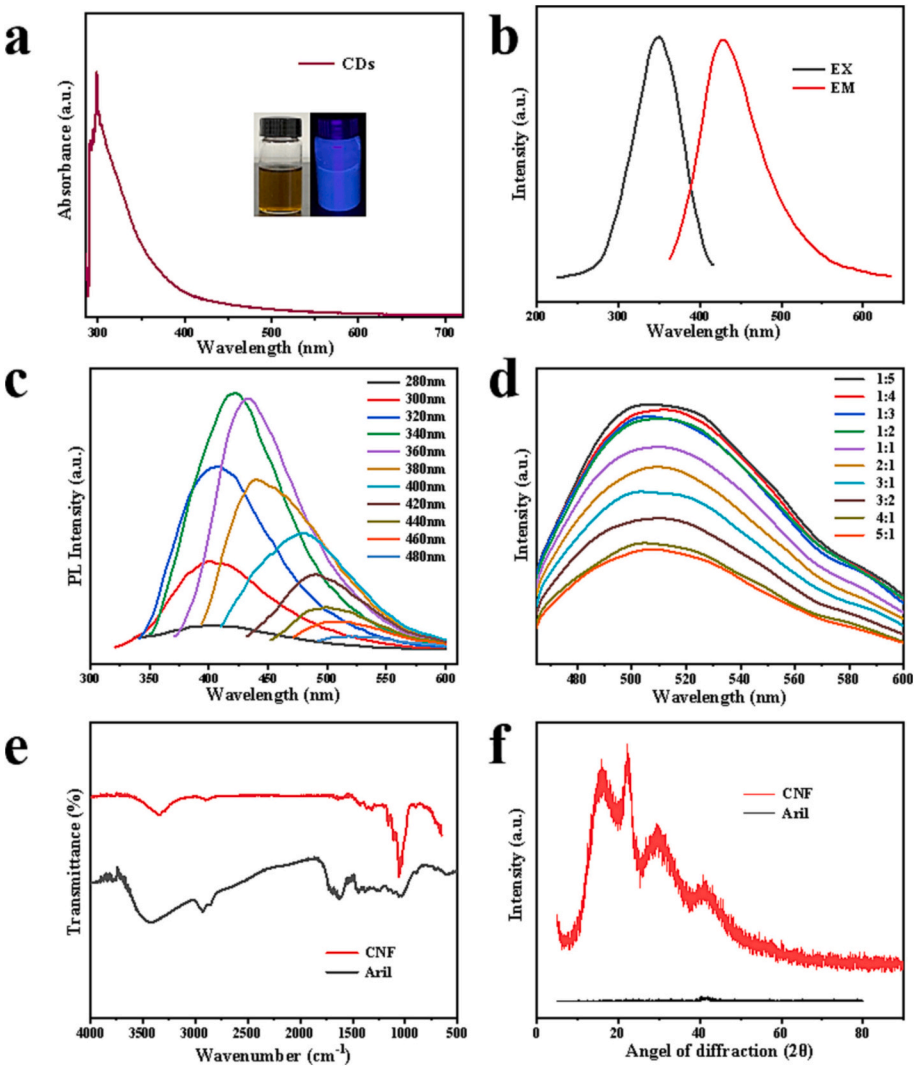

Fig. 2. UV–vis absorption (a), the insets show the image of CDs solution in visible light (left) and ultraviolet light (right); Photoluminescent spectra of CDs (b); Emission fluorescence spectra of CDs at different excitation wavelengths (c); Normalized fluorescence spectra of CDs of different concentrations (d), FTIR (e) and XRD (f) of the aril and CNF.

Table 1
The thickness and color parameters of the pure gelatin film and the CDs film with four adding ratios.

Film	Thickness(mm)	L	a	b	ΔE
G	0.05 ± 0.01^{a}	88.71 ± 1.33^{a}	-1.18 ± 0.25^{c}	9.64 ± 0.69^{c}	5.94 ± 1.30^{d}
G/5CD	0.05 ± 0.01^{a}	85.32 ± 0.44^{b}	-0.35 ± 0.14^{c}	15.74 ± 0.55^{b}	12.77 ± 0.68^{c}
G/10CD	0.05 ± 0.01^{a}	79.28 ± 1.90^{c}	1.74 ± 0.78^{b}	25.82 ± 3.12^{a}	24.62 ± 3.69^{b}
G/15CD	0.05 ± 0.02^{a}	76.68 ± 2.51^{cd}	2.8 ± 0.94^{ab}	27.76 ± 3.14^{a}	27.79 ± 4.08^{ab}
G/20CD	0.05 ± 0.01^{a}	74.62 ± 3.93^{d}	3.65 ± 1.81^{a}	29.02 ± 4.64^{a}	30.12 ± 6.26^{a}

* G: pure gelatin, G/5CD: pure gelatin with 5 % carbon dots, G/10CD: pure gelatin with 10 % carbon dots, G/15CD: pure gelatin with 15 % carbon dots, G/20CD: pure gelatin with 20 % carbon dots. The values indicate mean ± standard deviation. Different letters indicate significant statistical differences among the composite films with different levels of CDs mixtures ($P < 0.05$).

reduction in clarity and transparency of the film [39]. Results showed that the surface of G/10CD/3CNF, G/10CD/5CNF and G/10CD/7CNF films were rough due to the addition of CNF. To better understand the morphology of the composite films, the plane and cross-section were observed using SEM. Results showed that the surface and cross-section of both G and G/10CD films were relatively smooth, with CDs not appearing to affect G film morphology (Fig. 4a1-b1 and a2-b2). Compared with G and G/10CD, the surface of G/10CD/5CNF and G/10CD/7CNF films were uneven and convex, with a rougher section (Fig. 4d1-e1 and d2-e2), indicating that CNF was embedded inside the film.

The thickness of G film decreased after CDs addition (Table 2), suggestive that CDs were tightly filled in gelatin film. Compared with G/10CD film, the thickness of the composite films (G/10CD/3CNF, G/10CD/5CNF, and G/10CD/7CNF) were significantly higher after the addition of CNF ($P < 0.05$), concurrent with increased thickness increased with CNF addition. The thicker composite film was attributed to the more solid matter additions [34].

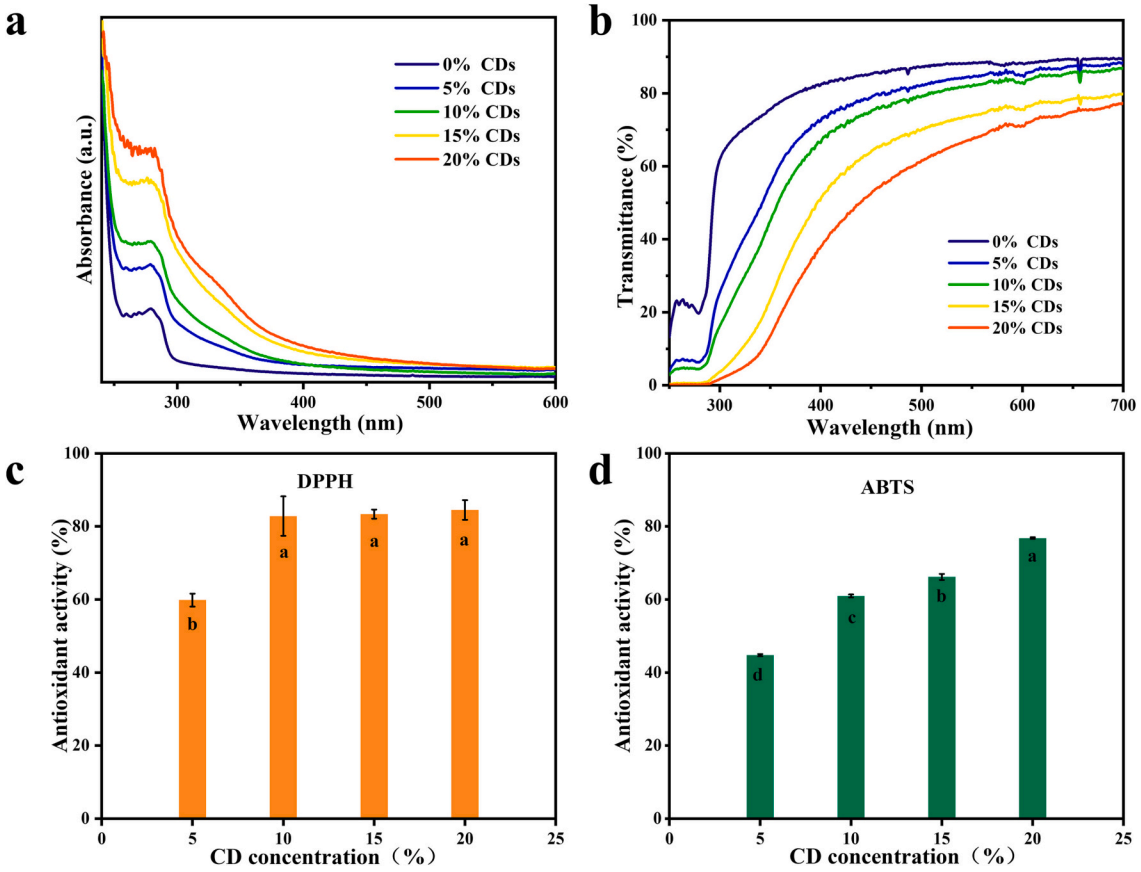

Fig. 3. Different proportions of gelatin film absorption curve (a) and transmission curve (b); Free radical scavenging efficiency with different CDs content in DPPH (c) and ABTS method (d). *G: pure gelatin, G/5CD: pure gelatin mixed with 5 % carbon dots, G/10CD: pure gelatin mixed with 10 % carbon dots, G/15CD: pure gelatin mixed with 15 % carbon dots, G/20CD: pure gelatin mixed with 20 % carbon dots. The values indicate mean ± standard deviation. Different letters indicate significant statistical differences among the composite films with different levels of CDs mixtures ($P < 0.05$).

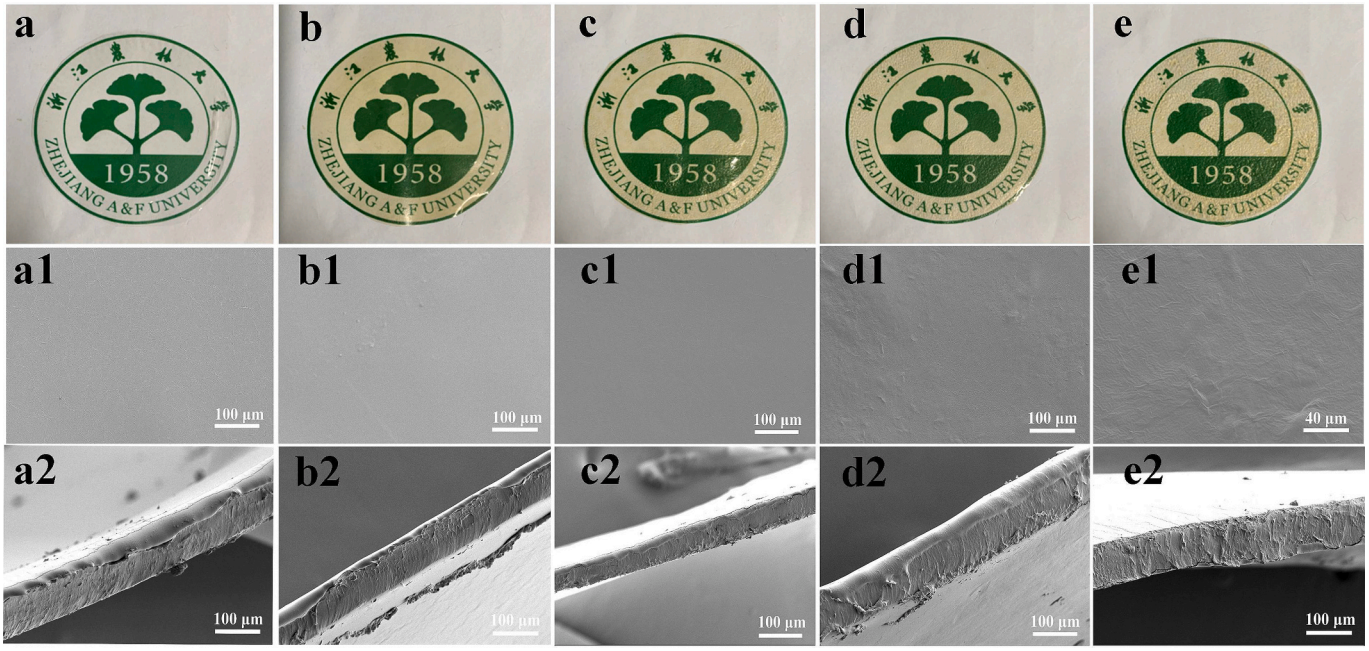

Fig. 4. Image of the transparent appearance (a-e), SEM micrographs surface (a1-e1) and the cross-section (a2-e2) of G, G/10CD, G/10CD/3CNF, G/10CD/5CNF, G/10CD/7CNF.

Table 2
The thickness, water vapor transmittance, water solubility and moisture content of the five membranes.

Film	Thickness (mm)	WVP ($\times 10^{-10}$ g/m^{2}hPa)	WS (%)	MC (%)
G	0.09 ± 0.01^{c}	7.48 ± 0.42^{a}	70.32 ± 11.99^{a}	7.42 ± 1.9^{a}
G/10CD	0.07 ± 0.01^{d}	6.28 ± 2.51^{ab}	65.23 ± 10.5^{a}	6.7 ± 0.64^{a}
G/10CD/3CNF	0.12 ± 0.01^{b}	1.84 ± 1.23^{b}	53.76 ± 12.28^{ab}	6.56 ± 0.82^{a}
G/10CD/5CNF	0.14 ± 0.02^{a}	5.61 ± 4.26^{ab}	55.69 ± 12.05^{a}	6.78 ± 0.13^{a}
G/10CD/7CNF	0.15 ± 0.01^{a}	7.08 ± 2.58^{ab}	31.76 ± 16.23^{b}	6.04 ± 0.92^{a}

* G: pure gelatin, G/10CD: pure gelatin with 10 % carbon dots, G/10CD/3CNF: pure gelatin with 10 % carbon dots and 3 % cellulose nanofibers, G/10CD/5CNF: pure gelatin with 10 % carbon dots and 5 % cellulose nanofibers, G/10CD/7CNF: pure gelatin with 10 % carbon dots and 7 % cellulose nanofibers, WVP: water vapor permeability, WS: water solubility, MC: moisture content. The values indicate mean ± standard deviation, different letters indicate significant statistical differences ($P < 0.05$).

3.4. Fourier transform infrared spectroscopy (FTIR) and X-ray diffraction (XRD) of G/10CD/CNF films

The functional groups in CNF and G, G/10CD, G/10CD/CNF films were analyzed by FTIR spectroscopy, respectively (Fig. 5a) to account for reaction outcomes in film preparation. Absorption band at 3340 cm^{-1} was observed in all film samples corresponding to the stretching vibration of O—H [40] and that of -NH_2 in gelatin [41]. The position of 3340 cm^{-1} band became wider after incorporation of CDs and gelatin into CNF suggestive that was obvious interaction between CNF, CDs, and gelatin. In addition, two bands appearing at 2930 and 1650 cm^{-1} were found in G, G/CD and G/CD/CNF films, corresponding to the characteristic peaks of C—H [36] and C═O [11], respectively. The appearance of C═O was suggested to inder for protein secondary structure corresponding to amide I [25]. The band at 1161 cm^{-1} was only found in CNF and G/CD/CNF film attributed to typical polysaccharide functional group of C-O-C in CNF [42].

Considering the possible involvement of organic nanoparticles in film formation, XRD experiments was used to analyze the phase in G, G/CD and G/CD/CNF films (Fig. 5b). The diffraction peak in three films appearing at 19°, 30°and 41° revealed that the addition of CDs and CNF did not damage structure of gelatin, with the peak at 19° related to β-fold structure of gelatin [43]. Compared with G film, both the peak strength of G/CD and G/CD/CNF films significantly decreased, indicating that the addition of CDs and CNF could block gelatin original regular structure [44]. The damaged intramolecular associations started to recover with CNF addition as indicated by the higher band strength was in G/CD/CNF films compared with that in G/CD film.

3.5. Water barrier capacity and water resistance of G/CD/CNF films

Usually, food storage typically needs a dry environment, but also to keep water inside the food from evaporation, which requires a certain degree of water barrier packaging materials [45]. The water vapor permeability (WVP) is an index to assess film ability to allow for water diffusion in and outside [3]. As can be seen in Table 2, G/10CD/3CNF film showed maximum water barrier capacity (1.84 ± 1.23 × 10^{-10} g m/m^{2}hPa), much lower than the packaging of gelatin agar with nanofibers (0.56 ± 0.1 × 10^{-9} g/m^{2}sPa) [46]. However, WVP in case of G/10CD/5CNF and G/10CD/7CNF films significantly increased in comparison to G/10CD/3CNF film. Excess CNF inside the film would aggregate and change the water transport path inside the film [47].

The water solubility (WS) of G/10CD/7CNF film was significantly lower than that of other films likely attributed to CNF hydrophobicity [48]. There is no significant differences in moisture content (MC) among all the samples. In addition, the changes in the water contact angle (WCA) of the five films were within 55 s (Table 3). The WCA at 5 s for G and G/10CD films were at 54.5°and 47.6°, respectively, and decreased by 2.5° and 8.6° at 55 s. Decrease in WCA in case of G/CD compared with G is attributed to CDs good water compatibility, making the gelatin

Table 3
Water contact angle of different membranes within a minute.

Film	Time		
	5 s	15 s	55 s
G	 54.5°	 53.1°	 52°
G/10CD	 47.6°	 45°	 38°
G/10CD/3CNF	 59.3°	 55.5°	 52.5°
G/10CD/5CNF	 62.5°	 62.5°	 62.4°
G/10CD/7CNF	 65.6°	 64.4°	 64°

* G: pure gelatin, G/10CD: pure gelatin with 10 % carbon dots, G/10CD/3CNF: pure gelatin with 10 % carbon dots and 3 % cellulose nanofibers, G/10CD/5CNF: pure gelatin with 10 % carbon dots and 5 % cellulose nanofibers, G/10CD/7CNF: pure gelatin with 10 % carbon dots and 7 % cellulose nanofibers.

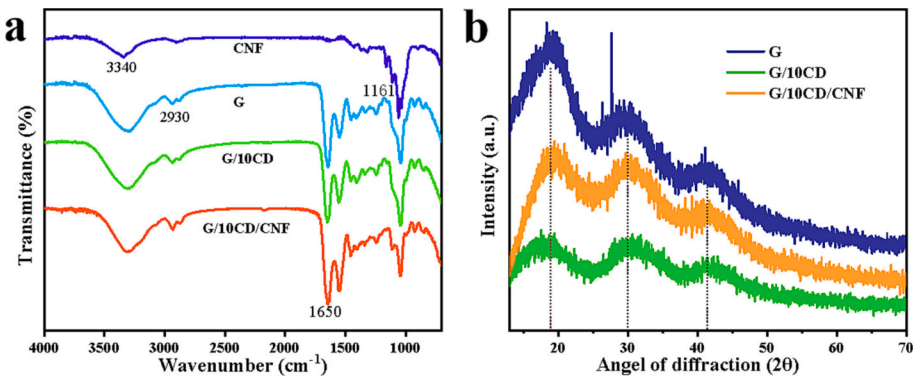

Fig. 5. The FTIR spectra (a) and XRD patterns (b) of different membranes.
*CNF: cellulose nanofibers; G, pure gelatin; G/10CD, pure gelatin mixed with 10 % carbon dots; G/10G/CNF, pure gelatin mixed with 10 % carbon dots and define CNF.

film more hydrophilic [49]. The initial WCA of G/10CD/3CNF, G/10CD/5CNF and G/10CD/7CNF films was significantly higher than that of G/10CD film ranging from 59.3° to 65.6°. Moreover, reduction of WCA for G/10CD/3CNF, G/10CD/5CNF and G/10CD/7CNF films was less than that for G/CD during 5 s to 55 s, indicating that gelatin film mixed with CDs and CNF exerted better surface hydrophobicity. Our result was consistent with previous report that the addition of CNF makes the membrane structure more compact, and the internal molecules were cross-linked, effectively reducing its hydrophilicity [50].

3.6. Thermal and mechanical properties of films

As shown in Fig. 6, weight loss of film sample can be divided into three steps. The first change in weight loss occurred between 30 °C and 128 °C for the five film samples, which mainly corresponded to water evaporation [51]. The second stage ranged from 130 to 217 °C, the weight loss of all samples corresponded to the decomposition of glycerol [52]. The maximum weight loss began after 250 °C (corresponding to the third stage), which was mainly attributed to the degradation of gelatin macromolecule [53]. Interestingly, percentages of weight loss of G/10CD/3CNF, G/10CD/5CNF, and G/10CD/7CNF films were less than those of G and G/10CD films during whole stage, indicating CNF addition blocks moisture and combines with gelatin to form a tighter reticular membrane, improving the thermal stability of the membrane [9].

Pure gelatin films often need to be improved by adding fillers due to its poor mechanical properties. Compared with G film, the tensile strength of G/10CD film sharply decreased by 3 MPa after incorporation of CDs (Table 4), and with an increase of 170 % in elongation at break (Table 4 and Fig. 6b), which may be explained that G/10CD film absorbs moisture in the air and greatly improves the film toughness [54]. The elongation at break of G/10CD film significantly decreased when mixed with CNF. In contrast, the tensile strength of G/10CD film showed an increasing trend after mixing with 3 wt% CNF or 5 wt% CNF. Decrease in tensile strength of G/10CD/5CNF film may be due to the aggregation of CNF inside the film [9]. Altogether the G/10CD/3CNF film exerted better mechanical property among the three composite films (G/10CD/3CNF, G/10CD/5CNF and G/10CD/7CNF).

Table 4
Tensile strength and elongation at break of different films.

Film	Tensile strength(MPa)	Elongation at break(%)
G	10.83	30
G/10CD	7.83	200
G/10CD/3CNF	9.09	120
G/10CD/5CNF	8.10	140
G/10CD/7CNF	6.41	126

* G: pure gelatin, G/10CD: pure gelatin with 10 % carbon dots, G/10CD/3CNF: pure gelatin with 10 % carbon dots and 3 % cellulose nanofibers, G/10CD/5CNF: pure gelatin with 10 % carbon dots and 5 % cellulose nanofibers, G/10CD/7CNF: pure gelatin with 10 % carbon dots and 7 % cellulose nanofibers.

3.7. Antibacterial activity of G/10CD/3CNF/EON film

Fresh fruits infected with *E. coli* can lead to the outbreak of foodborne diseases [55]. Several studies showed that essential oils could inhibit *E. coli* likely attributed for its richness in phenols [56] and terpenes [57]. The inhibition ability of the composite membrane solution after incorporation of essential oil to *E. coli* was evaluated using the plate counting method. As can be seen from Fig. 7, the bactericidal effect could not be achieved by the reaction of the membrane fluid with the bacteria for 2 h, whereas the number of colonies gradually decreased after 3 h, indicating that the essential oil wrapped by the active agent in the membrane fluid was gradually released.

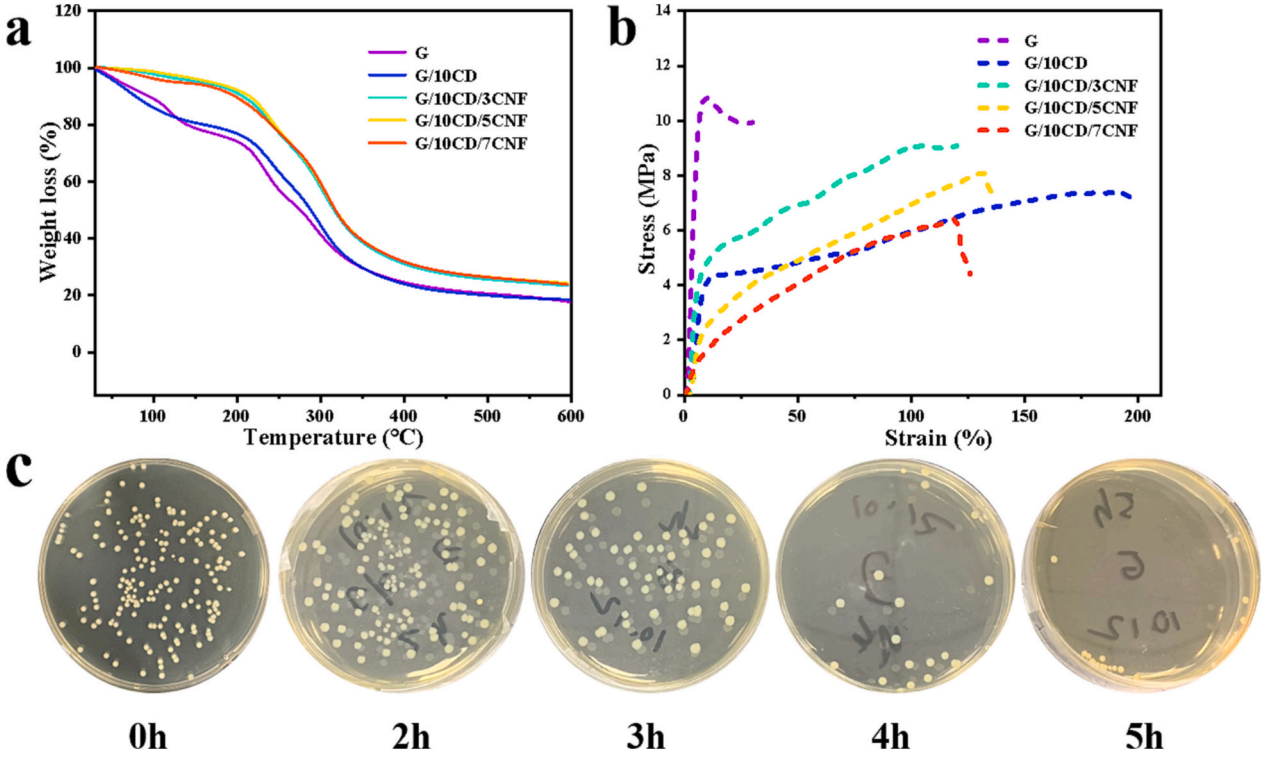

Fig. 6. The thermogravimetric (a) and mechanical properties (b) of five membranes, and inhibition effect of NEO in membrane fluid on *E. coli* within different reaction time (c) *G: pure gelatin; G/10CD: pure gelatin mixed with 10 % carbon dots; G/10CD/3CNF: pure gelatin mixed with 10 % carbon dots and 3 % cellulose nanofibers; G/10CD/5CNF: pure gelatin mixed with 10 % carbon dots and 5 % cellulose nanofibers; G/10CD/7CNF: pure gelatin mixed with 10 % carbon dots and 7 % cellulose nanofibers.

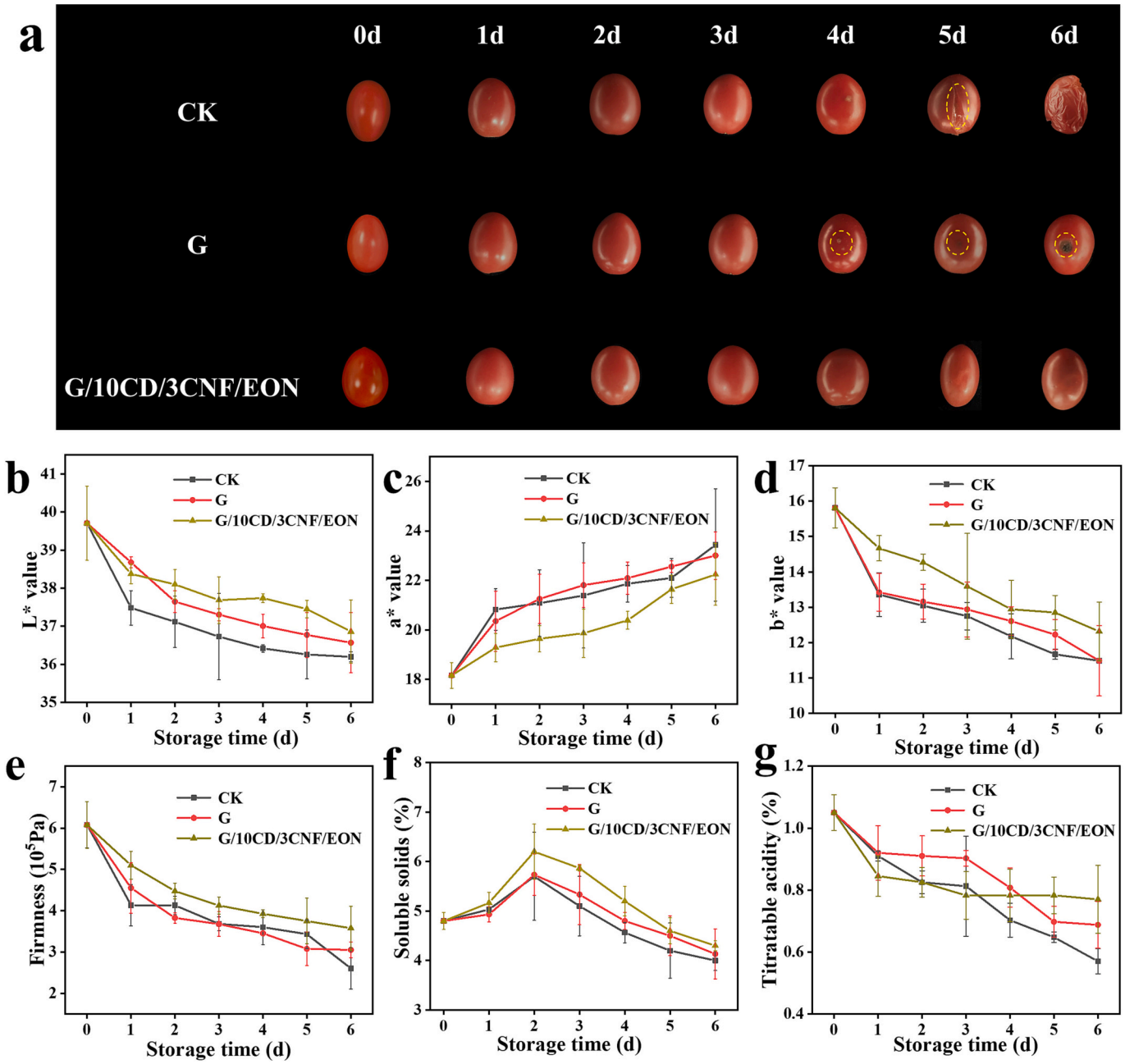

Fig. 7. Changes in the appearance (a), L* value (b), a* value (c), b* value (d), hardness (e), soluble solids content (f), titratable acidity (g) of tomatoes with different coating films during storage stage. *CK: control tomato; G: the tomato coating by the pure gelatin film; G/10CD/3CNF/EON, the tomato coating by the pure gelatin mixed with 10 % carbon dots, 3 % cellulose nanofibers and nanoemulsions of essential oil.

3.8. The application of G/10CD/3CNF/EON film on tomato storage

The changes in appearance of tomatoes within 6 d of storage under different treatments are shown in Fig. 7. The tomato in control group became soft and showed a pericarp rupture at 5 d of storage. The pure gelatin coating tomatoes remained intact in shape but with moldy during the whole storage. In contrast, the tomatoes maintained their intact shape without moldy, indicating that G/10CD/3CNF/EON exerted efficient antibacterial activity, which aided tomatoes to maintain good quality under the same conditions.

The change of tomatoes color reflects its maturity and quality to some extent. The lightness and yellowness of tomatoes in each group showed decrease trend during storage, whereas redness showed continuously increase (Fig. 7). The tomatoes treated with G/10CD/3CNF/EON showed better lightness and yellowness, but lower redness, which indicating that the composite film can maintain the good appearance of tomato under the same conditions.

The tomato belongs to the respiration jump type fruit, after the mature period of storage, will carry on the oxygen-free respiration to consume the substrate [58]. The firmness of tomato in each group gradually decreased during storage, the reduction in hardness was slower in case of G/10CD/3CNF/EON group than in CK, indicating that the complex film wrapped around tomato to form a barrier, and aid to maintain the fruit hardness by reducing water loss.

Soluble solids (SS) and titratable acid (TA) are the key indicators for fruit quality assessment [59]. It can be seen from the Fig. 7e that the SS in each group began to decrease after 2 d likely explained to soluble polysaccharides decomposition to monosaccharides, ultimately leading

to fruit deterioration [60]. Similarly, TA in each group showed a decreasing trend during storage, indicating the organic acids were consumed by anaerobic respiration. In the present study, reduction of SS in G/10CD/3CNF/EON group was less than that observed in case of G and control for most days during storage. The tomato in G/10CD/3CNF/EON group maintained higher TA at the late stage during storage.

4. Conclusion

In summary, a biodegradable, sustainable, anti-microbial and flexible nanocoposite for fruits coating was successfully developed using the waste fish scale and the aril of *T. grandis* waste products. The G/10CD film exhibited significantly improved UV absorption and antioxidant capacity compared with pure gelatin film, with significantly lower water vapor permeability (WVP), water contact angle (WCA) and lower tensile strength (TS). However, G/10CD film showed an improved WVP, WCA and TS of G/10CD film after incorporation of 3 wt% CNF. The G/10CD/3CNF film exerted anti-microbial ability for *Escherichia coli* by addition of EON. Furthermore, G/10CD/3CNF/EON film was also demonstrated that can effectively prolong tomato shelf life. Therefore, such multifunctional and low-cost gelatin-based film shows great potential in tomato packaging and has yet to be examined for other food products. In addition, primary materials used in production of these biofilms were derived from the most abundant biopolymers, which can powerfully solve the problems of agricultural waste (such as fish scale and the aril of *T. grandis*).

CRediT authorship contribution statement

Jiasheng Wu, Dapeng Yang, and Lili Song designed the work. Junjun Bao, Yuanyuan Hu and Weiwei Huan did running the experiments and data analysis and statistics. Junjun Bao, Yuanyuan Hu, and Mohamed A Farag did the article writing and revising. All authors contributed to the article and approved the submitted manuscript.

Declaration of competing interest

The authors declare no conflict of interest.

Data availability

The data that has been used is confidential.

Acknowledgements

This work was financially supported by the Key Research and Development Program of Zhejiang Province (2021C02013), the Zhejiang Provincial Cooperative Forestry Science and Technology Project (2021SY01).

References

[1] M. Kan, S.A. Miller, Environmental impacts of plastic packaging of food products, Resour. Conserv. Recycl. 180 (2022), 106156.
[2] X. Li, Y. Wei, S. Jiang, Y. Zhou, J. Li, K. Li, S.Q. Shi, J. Li, Full bio-based soy protein isolate film enhanced by chicken feather keratin, Macromol. Mater. Eng. 306 (5) (2021) 2100004.
[3] J.-W.R. Shiv Shankar, Preparation of sulfur nanoparticle-incorporated antimicrobial chitosan films, Food Hydrocoll. 82 (2018) 116–123.
[4] L. Fernández-de Castro, M. Mengíbar, Á. Sánchez, L. Arroyo, M.C. Villarán, E. Díaz de Apodaca, Á. Heras, Films of chitosan and chitosan-oligosaccharide neutralized and thermally treated: effects on its antibacterial and other activities, LWT Food Sci. Technol. 73 (2016) 368–374.
[5] S. Phadtare, V. D'Britto, A. Pundle, A. Prabhune, M. Sastry, Invertase-lipid biocomposite films: preparation, characterization, and enzymatic activity, Biotechnol. Prog. 20 (2004) 156–161.
[6] N. Thongsrikhem, S. Taokaew, M. Sriariyanun, S. Kirdponpattara, Antibacterial activity in gelatin-bacterial cellulose composite film by thermally crosslinking with cinnamaldehyde towards food packaging application, Food Packag. Shelf Life 31 (2022), 100766.
[7] G. Mondragon, C. Peña-Rodriguez, A. González, A. Eceiza, A. Arbelaiz, Bionanocomposites based on gelatin matrix and nanocellulose, Eur. Polym. J. 62 (2015) 1–9.
[8] S. Lv, L. Hu, C. Xia, M.B. Cabrera, Y. Guo, C. Liu, L. You, Recycling fish scale powder in improving the performance of asphalt: a sustainable utilization of fish scale waste in asphalt, J. Clean. Prod. 288 (2021), 125682.
[9] W. Wang, Y. Liu, H. Jia, Y. Liu, H. Zhang, Z. He, Y. Ni, Effects of cellulose nanofibers filling and palmitic acid emulsions coating on the physical properties of fish gelatin films, Food Biophys. 12 (1) (2016) 23–32.
[10] L. Pan, P. Li, Y. Tao, Preparation and properties of microcrystalline cellulose/fish gelatin composite film, Materials 13 (19) (2020) 4370.
[11] E. Farshchi, S. Pirsa, L. Roufegarinejad, M. Alizadeh, M. Rezazad, Photocatalytic/biodegradable film based on carboxymethyl cellulose, modified by gelatin and TiO2-Ag nanoparticles, Carbohydr. Polym. 216 (2019) 189–196.
[12] Y. Wang, A. Hu, Carbon quantum dots: synthesis, properties and applications, J. Mater. Chem. C 2 (34) (2014) 6921–6939.
[13] X. Zhang, H. Wang, C. Ma, N. Niu, Z. Chen, S. Liu, J. Li, S. Li, Seeking value from biomass materials: preparation of coffee bean shell-derived fluorescent carbon dots via molecular aggregation for antioxidation and bioimaging applications, Mater. Chem. Front. 2 (7) (2018) 1269–1275.
[14] V. Kumar, A. Elfving, H. Koivula, D. Bousfield, M. Toivakka, Roll-to-roll processed cellulose nanofiber coatings, Ind. Eng. Chem. Res. 55 (12) (2016) 3603–3613.
[15] R. Das, T. Lindstrom, P.R. Sharma, K. Chi, B.S. Hsiao, Nanocellulose for sustainable water purification, Chem. Rev. 122 (9) (2022) 8936–9031.
[16] A. Ali, Y. Chen, H. Liu, L. Yu, Z. Baloch, S. Khalid, J. Zhu, L. Chen, Starch-based antimicrobial films functionalized by pomegranate peel, Int. J. Biol. Macromol. 129 (2019) 1120–1126.
[17] Y. Zhang, Y. Liu, R. Li, X. Ren, T.S. Huang, Preparation and characterization of antimicrobial films based on nanocrystalline cellulose, J. Appl. Polym. Sci. 136 (8) (2018) 47101.
[18] M. Nasiri, H. Ahari, A. Sharifan, A.A. Anvar, S. Kakolaki, Nanoemulsion production techniques upgrade bioactivity potential of nanoemulsified essential oils on Acipenser stellatus filet preserving, Int. J. Food Prop. 23 (1) (2020) 2174–2188.
[19] X. Feng, W. Wang, Y. Chu, C. Gao, Q. Liu, X. Tang, Effect of cinnamon essential oil nanoemulsion emulsified by OSA modified starch on the structure and properties of pullulan based films, LWT Food Sci. Technol. 134 (2020).
[20] S. He, X. Ren, Y. Lu, Y. Zhang, Y. Wang, L. Sun, Microemulsification of clove essential oil improves its *in vitro* and *in vivo* control of *Penicillium digitatum*, Food Control 65 (2016) 106–111.
[21] J. Wu, J. Huang, Y. Hong, H. Zhang, M. Ding, H. Lou, Y. Hu, W. Yu, L. Song, De novo transcriptome sequencing of *Torreya grandis* reveals gene regulation in sciadonic acid biosynthesis pathway, Ind. Crop. Prod. 120 (2018) 47–60.
[22] J.J. Cui, W.J. Li, C.L. Wang, Y.Q. Huang, W. Lin, B. Zhou, J.M. Yue, Antimicrobial abietane-type diterpenoids from *Torreya grandis*, Phytochemistry 201 (2022), 113278.
[23] Y.-J. Yu, S. Ni, F. Wu, W.-G. Sang, Chemical composition and antioxidant activity of essential oil from *Torreya grandis* cv.merrillii arils, J. Essent. Oil Bear. Pl. 19 (5) (2016) 1170–1180.
[24] A. Farooq, M.K. Patoary, M. Zhang, H. Mussana, M. Li, M.A. Naeem, M. Mushtaq, A. Farooq, L. Liu, Cellulose from sources to nanocellulose and an overview of synthesis and properties of nanocellulose/zinc oxide nanocomposite materials, Int. J. Biol. Macromol. 154 (2020) 1050–1073.
[25] L.S.F. Leite, C.M. Ferreira, A.C. Correa, F.K.V. Moreira, L.H.C. Mattoso, Scaled-up production of gelatin-cellulose nanocrystal bionanocomposite films by continuous casting, Carbohydr. Polym. 238 (2020), 116198.
[26] Y. Yuan, H. Chen, Preparation and characterization of a biodegradable starch-based antibacterial film containing nanocellulose and polyhexamethylene biguanide, Food Packag. Shelf Life 30 (2021), 100718.
[27] Y. Wang, C. Cen, J. Chen, C. Zhou, L. Fu, Nano-emulsification improves physical properties and bioactivities of litsea cubeba essential oil, LWT Food Sci. Technol. 137 (2021), 110361.
[28] G. Chellasamy, S.K. Arumugasamy, S. Govindaraju, K. Yun, Green synthesized carbon quantum dots from maple tree leaves for biosensing of cesium and electrocatalytic oxidation of glycerol, Chemosphere 287 (2022), 131915.
[29] W.A. Amer, A.F. Rehab, M.E. Abdelghafar, N.L. Torad, A.S. Atlam, M.M. Ayad, Green synthesis of carbon quantum dots from purslane leaves for the detection of formaldehyde using quartz crystal microbalance, Carbon 179 (2021) 159–171.
[30] S. Elanthikkal, T. Francis, S. Akhtar, Utilization of areca nut leaf sheath fibers for the extraction of cellulose whiskers, J. Nat. Fibers 18 (9) (2019) 1261–1273.
[31] H.V.L.a.S.B.A.H, Y. Mazlita, Preparation of cellulose nanocrystals bio-polymer from agro-industrial wastes: separation and characterization, Polym. Polym. Compos. 24 (9) (2016) 719–728.
[32] M.S. Abdel Aziz, H.E. Salama, Development of alginate-based edible coatings of optimized UV-barrier properties by response surface methodology for food packaging applications, Int. J. Biol. Macromol. 212 (2022) 294–302.
[33] X. Ye, R. Liu, X. Qi, X. Wang, Y. Wang, Q. Chen, X. Gao, Preparation of bioactive gelatin film using semi-refined pectin reclaimed from blueberry juice pomace: creating an oxidation and light barrier for food packaging, Food Hydrocoll. 129 (2022), 107673.
[34] S. Roy, P. Ezati, J.-W. Rhim, Gelatin/carrageenan-based functional films with carbon dots from enoki mushroom for active food packaging applications, ACS Appl. Polym. Mater. 3 (12) (2021) 6437–6445.
[35] L. Zhao, M. Zhang, A.S. Mujumdar, B. Adhikari, H. Wang, Preparation of a novel carbon dot/polyvinyl alcohol composite film and its application in food preservation, ACS Appl. Mater. Interfaces 14 (33) (2022) 37528–37539.

[36] L. Wang, Y. Wang, H. Wang, G. Xu, A. Doring, W.A. Daoud, J. Xu, A.L. Rogach, Y. Xi, Y. Zi, Carbon dot-based composite films for simultaneously harvesting raindrop energy and boosting solar energy conversion efficiency in hybrid cells, ACS Nano 14 (8) (2020) 10359–10369.
[37] E. Jamroz, P. Kopel, J. Tkaczewska, D. Dordevic, S. Jancikova, P. Kulawik, V. Milosavljevic, K. Dolezelikova, K. Smerkova, P. Svec, V. Adam, Nanocomposite furcellaran films-the influence of nanofillers on functional properties of furcellaran films and effect on linseed oil preservation, Polymers 11 (12) (2019) 2046.
[38] H. Wang, Y. Xie, X. Na, J. Bi, S. Liu, L. Zhang, M. Tan, Fluorescent carbon dots in baked lamb: formation, cytotoxicity and scavenging capability to free radicals, Food Chem. 286 (2019) 405–412.
[39] S.R. Djafari Petroudy, E. Rasooly Garmaroody, H. Rudi, Oriented cellulose nanopaper (OCNP) based on bagasse cellulose nanofibrils, Carbohydr. Polym. 157 (2017) 1883–1891.
[40] J.M. Fonseca, G.A. Valencia, L.S. Soares, M.E.R. Dotto, C.E.M. Campos, R. Moreira, A.R.M. Fritz, Hydroxypropyl methylcellulose-TiO_2 and gelatin-TiO_2 nanocomposite films: physicochemical and structural properties, Int. J. Biol. Macromol. 151 (2020) 944–956.
[41] K. Li, S. Jin, H. Chen, J. Li, Bioinspired interface engineering of gelatin/cellulose nanofibrils nanocomposites with high mechanical performance and antibacterial properties for active packaging, Compos. B. Eng. 171 (2019) 222–234.
[42] Y. Yao, H. Wang, R. Wang, Y. Chai, W. Ji, Fabrication and performance characterization of the membrane from self-dispersed gelatin-coupled cellulose microgels, Cellulose 26 (5) (2019) 3255–3269.
[43] A. Ahmadi, P. Ahmadi, M.A. Sani, A. Ehsani, B. Ghanbarzadeh, Functional biocompatible nanocomposite films consisting of selenium and zinc oxide nanoparticles embedded in gelatin/cellulose nanofiber matrices, Int. J. Biol. Macromol. 175 (2021) 87–97.
[44] X. Su, Z. Yang, K.B. Tan, J. Chen, J. Huang, Q. Li, Preparation and characterization of ethyl cellulose film modified with capsaicin, Carbohydr. Polym. 241 (2020), 116259.
[45] P. Ezati, J.-W. Rhim, R. Molaei, Z. Rezaei, Carbon quantum dots-based antifungal coating film for active packaging application of avocado, Food Packag. Shelf Life 33 (2022), 100878.
[46] S. Roy, J.-W. Rhim, Gelatin/agar-based functional film integrated with pickering emulsion of clove essential oil stabilized with nanocellulose for active packaging applications, Colloids Surf. Physicochem. Eng. Aspects 627 (2021), 127220.
[47] S. Mohammadalinejhad, H. Almasi, M. Esmaiili, Physical and release properties of poly(lactic acid)/nanosilver-decorated cellulose, chitosan and lignocellulose nanofiber composite films, Mater. Chem. Phys. 268 (2021), 124719.
[48] X. Zhang, Y. Li, M. Guo, T.Z. Jin, S.A. Arabi, Q. He, B.B. Ismail, Y. Hu, D. Liu, Antimicrobial and UV blocking properties of composite chitosan films with curcumin grafted cellulose nanofiber, Food Hydrocoll. 112 (2021), 106337.
[49] Z. Riahi, J.-W. Rhim, R. Bagheri, G. Pircheraghi, E. Lotfali, Carboxymethyl cellulose-based functional film integrated with chitosan-based carbon quantum dots for active food packaging applications, Prog. Org. Coat. 166 (2022), 106794.
[50] P. Taheri, R. Jahanmardi, M. Koosha, S. Abdi, Physical, mechanical and wound healing properties of chitosan/gelatin blend films containing tannic acid and/or bacterial nanocellulose, Int. J. Biol. Macromol. 154 (2020) 421–432.
[51] W. Ren, T. Qiang, L. Chen, Recyclable and biodegradable pectin-based film with high mechanical strength, Food Hydrocoll. 129 (2022), 107643.
[52] M. Tavassoli, M.A. Sani, A. Khezerlou, A. Ehsani, D.J. McClements, Multifunctional nanocomposite active packaging materials: immobilization of quercetin, lactoferrin, and chitosan nanofiber particles in gelatin films, Food Hydrocoll. 118 (2021), 106747.
[53] P. Wang, Y. Li, C. Zhang, F. Feng, H. Zhang, Sequential electrospinning of multilayer ethylcellulose/gelatin/ethylcellulose nanofibrous film for sustained release of curcumin, Food Chem. 308 (2020), 125599.
[54] M. Das Purkayastha, A.K. Manhar, V.K. Das, A. Borah, M. Mandal, A.J. Thakur, C. L. Mahanta, Antioxidative, hemocompatible, fluorescent carbon nanodots from an "end-of-pipe" agricultural waste: exploring its new horizon in the food-packaging domain, J. Agric. Food Chem. 62 (20) (2014) 4509–4520.
[55] D. Gupta, C.A. Madramootoo, Fate and transport of Escherichia coli in tomato production, Expos. Health 9 (2017) 13–25.
[56] I. Bassanetti, M. Carcelli, A. Buschini, S. Montalbano, G. Leonardi, P. Pelagatti, G. Tosi, P. Massi, L. Fiorentini, D. Rogolino, Investigation of antibacterial activity of new classes of essential oils derivatives, Food Control 73 (2017) 606–612.
[57] H. Yazgan, Y. Ozogul, E. Kuley, Antimicrobial influence of nanoemulsified lemon essential oil and pure lemon essential oil on food-borne pathogens and fish spoilage bacteria, Int. J. Food Microbiol. 306 (2019), 108266.
[58] W. Wang, D. Fan, Q. Hao, W. Jia, Signal transduction in non-climacteric fruit ripening, Hortic Res. 9 (2022) uhac190.
[59] Y. Zhu, D. Li, T. Belwal, L. Li, H. Chen, T. Xu, Z. Luo, Effect of nano-SiOx/chitosan complex coating on the physicochemical characteristics and preservation performance of green tomato, Molecules 24 (24) (2019) 4552.
[60] F. Xiang, Y. Xia, Y. Wang, Y. Wang, K. Wu, X. Ni, Preparation of konjac glucomannan based films reinforced with nanoparticles and its effect on cherry tomatoes preservation, Food Packag. Shelf Life 29 (2021), 100701.